P5.15 INVESTIGATING INTER-SATELLITE CALIBRATION FOR THE GPM ERA

F. Joseph Turk
Marine Meteorology Division, Naval Research Laboratory, Monterey, California 93943

S.W. Bidwell and Eric A. Smith
NASA-Goddard Space Flight Center, Greenbelt, Maryland 20771

Alberto Mugnai
CNR-Institute of Atmospheric and Climate Sciences, Frascati, Italy

1. INTRODUCTION

The Global Precipitation Measurement (GPM) is an international effort led by the National Aeronautics and Space Administration (NASA) of the USA and the National Space Development Agency of Japan (NASDA) for the purpose of improving climate, weather, and hydrological forecasts through more frequent and more accurate satellite measurement of precipitation globally. GPM will incorporate and assimilate data streams from many constellation spacecraft with varied orbital characteristics and instrument capabilities. A core satellite, the heart of GPM, will carry a Dual-frequency Precipitation Radar (DPR) and a conical scanning microwave radiometer, the GPM Microwave Imager (GMI). The GMI has many channels similar to the current Tropical Rainfall Measuring Mission (TRMM) Microwave Imager (TMI) and the Special Sensor Microwave Imagers (SSMI). The passive microwave channels and the two radar frequencies of the core are carefully chosen for investigating the varying character of precipitation over ocean and land, and from the tropics to the high-latitudes. With its unique instrument capabilities and inclined orbit, the core spacecraft will serve as a calibration 'transfer standard' to the remainder of the GPM constellation. In preparation, inter-satellite comparisons using the Tropical Rainfall Measuring Mission (TRMM) with the sun-synchronous SSMI radiometers have been conducted. We demonstrate a possible strategy for an inter-satellite calibration and transfer technique of the GPM constellation using realtime data from the TMI (serving as the core radiometer) and several of the SSMI instruments. Observational intersections of the core with the constellation spacecraft are essential in applying this technique to the member satellites. Information from core spacecraft retrievals during space-time orbital intersection events will be transferred to the constellation radiometer instruments in the form of improved calibration and, with experience, improved radiometric algorithms. Ongoing research involves study of critical variables in the inter-comparison, such as correlation with spatial-temporal separation of intersection events, frequency of intersection events, variable azimuth look angles, and variable resolution cells for the various sensors.

2. SIMULATING THE GPM

One objective of GPM is to provide enough sampling to reduce the uncertainty in short-term rainfall accumulations (Fleming, 2002; Bidwell et. al, 2002). This will require the various members of the GPM constellation to be synchronized such that their independently produced instantaneous precipitation estimates can be properly combined for global precipitation products at various space and time scales. In such a scenario, the core satellite would serve as a reference or calibration standard for all of the other constellation members. Each of the constellation members themselves will have very different sensors onboard (different channels, resolutions, etc.) and have different precipitation algorithms. The core serves as a transfer reference or standard, which would be applied when the core satellite encounters an intersection in its orbital pattern with a constellation member. While the details of the orbit configuration and how to transfer the calibration information to and from the core satellite have yet to be established (Smith et. al, 2001), there are a limited number of intersections of the core with any given constellation member. For monthly time scale rainfall products, this is much less of a concern than it is for the sub-daily time scale precipitation products. However, at sub-daily time scales and for spatial scales on the pixel level (0.25-degree or less), there will be a small number of overpasses relative to typical precipitating cloud lifetimes.

The current orbit pattern of the TRMM satellite (a west-to-east low-Earth tropical orbit, reaching up to approximately +/-40 degrees latitude) has a lower inclination than the proposed orbit inclination for the GPM core, yet it encounters many intersections with the various sun-synchronous, near-polar orbiting meteorological satellites, such as the Defense Meteorological Satellite Platform (DMSP) and the National Oceanic and Atmospheric Administration (NOAA) platforms. In order to simulate the GPM configuration, we examined three months of data

between November 2001 and February 2002, and extracted space- and time-collocated data points between the TMI and the SSMI aboard the F-13, 14, and 15 instruments. The three SSMI themselves are well inter-calibrated though extensive calibration-validation programs that took place after each DMSP launch (Hollinger et.al, 1990). Very-fine time and space coincident TMI-SSMI pixel pairs were extracted using a maximum allowed time and space offset of one-minute and 10-km, respectively. The one-minute time alignment assures that the TMI and SSMI are viewing the on-Earth location at the same time, so that when data are further averaged over larger spatial domains, the respective TMI and SSMI averages are near-coincident. These data were further separated into over-ocean and over-land pixels (coastal pixels were discarded), and no-rain and rain pixels depending upon the TMI 2A12 algorithm rain flag. In order to account somewhat for varying spatial resolution of the different instruments, the TMI data were averaged over a 3x3 box size (this is a crude first-order correction). While the TMI and SSMI both have approximately the same on-Earth incidence angle (53 degrees), the azimuthal viewing direction of each sensor is different, which forms the basis for the investigation below.

a) No-rain conditions.

Figure 1 depicts the observing conditions for idealized no-rain conditions (assuming that the TMI rain flag correctly indicated no rain). Over ocean, 19 GHz variations largely arise from ocean emissivity differences due to wind speed direction and magnitude, and the presence of clouds. At 85 GHz, the presence of water vapor increasingly masks the surface.

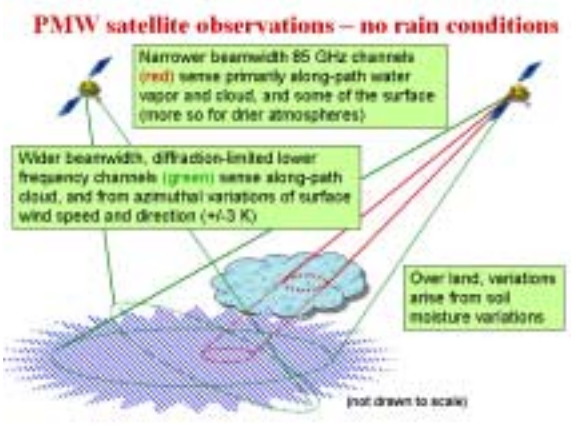

Figure 1. Some factors influencing the differences between space- and time-collocated TMI and SSMI observations under idealized no-rain conditions.

In Figure 2, we display the scatter plot of the six channels that are the same on the TMI and the SSMI (19V, 19H, 37V, 37H, 85V and 85H) where V and H refer to the vertical and horizontally-polarized channels at 19, 37 and 85 GHz, and all data represent pixels where the TMI rain flag indicated no rain.

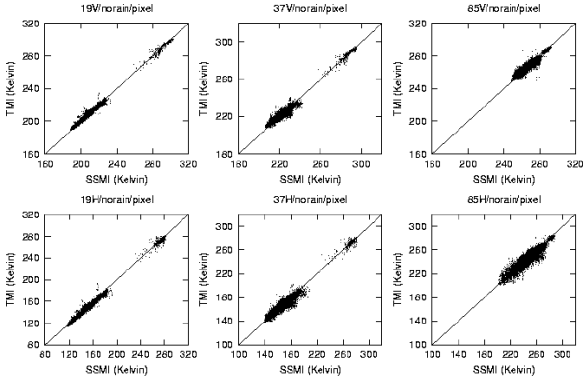

Figure 2. Scatter plot of time and space-coincident TMI and SSMI pixels under conditions where the TMI rain flag indicated no rain. Each point represents a TMI-SSMI pixel pair aligned to within 1-minute in time and within 10-km in space. **Top row**: 19V, 37V and 85V channels. **Bottom row**: 19H, 37H and 85H channels.

The points align themselves along the 1:1 line, but the scatter in the data is evidence of, among other things, variations in the presence of non-precipitating clouds in the different fields of view (FOV), and from differences arising from different azimuthal viewing directions of the same location as shown in Figure 1. The over-ocean and over-land points clump together, especially at 19 and 37 GHz, owing to the radiometrically cold and warm ocean and land surfaces, respectively. In order to verify that the collocation software was functioning properly, these data were further binned into the nearest 1-degree box and then averaged. Figure 3 depicts the results.

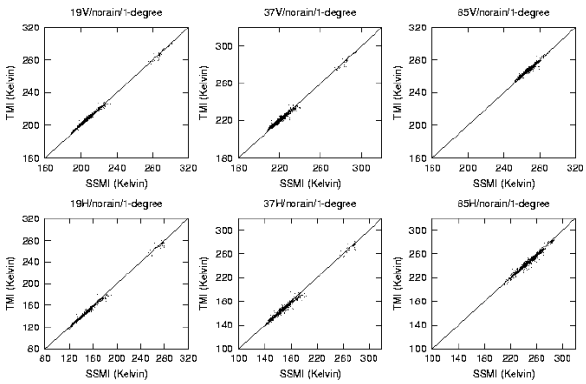

Figure 3. Same as Figure 2, but the data are further binned into their nearest 1-degree bin and averaged.

By averaging the collocated data into the 1-degree bins, much of the variation due to underlying wind speed (in the over-ocean case) and surface emissivity variations (in the over-land case) are averaged away. The data are very well correlated with no bias between the TMI and SSMI channels, although the cold end of the 85 GHz channels is not represented here. These data show that the no-rain, or quiescent conditions, are well correlated between the TMI and the SSMI. The next step is to perform similar studies between these data when the TMI rain flag indicated rain.

b) Raining conditions.

Figure 4 depicts the situation where a precipitating cloud is in the FOV of the TMI and the SSMI. Even with tight space and time alignments of the TMI and SSMI pixels, substantially different viewing geometries are presented to a passive microwave instrument, depending upon the three-dimensional structure of the cloud and the azimuthal direction that the sensor views it. Depending upon the relative azimuth difference between the TMI and SSMI viewing position, substantial brightness temperature differences may arise, especially at 85 GHz where the ice optical path is different (Vivekanandan et.al, 1991). While there have been several theoretical studies of the effect of three dimensional precipitating clouds upon microwave radiative transfer to space (Bauer et. al. 1998; Haferman et.al, 1993), there is very little observational data to verify and quantify the effects of three-dimensional precipitating clouds when viewed along different directions.

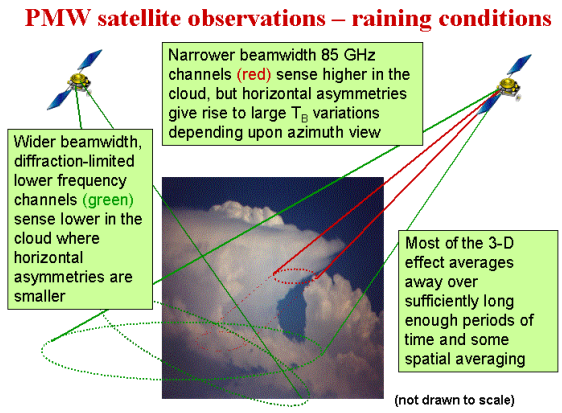

Figure 4. Some factors influencing the differences between space- and time-collocated TMI and SSMI observations under idealized precipitating cloud conditions.

Figure 5 depicts the same plot as Figure 2, except for conditions where the TMI rain flag indicated rain.

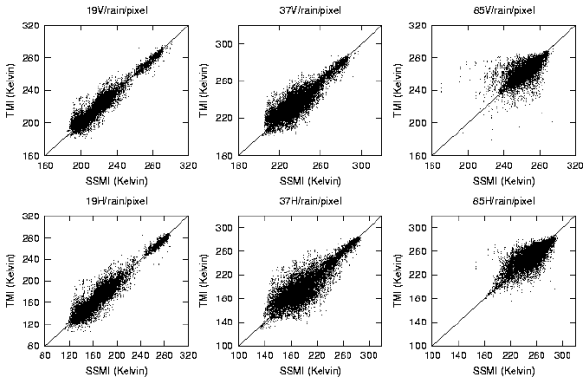

Figure 5. Same as Figure 2, except for collocated TMI-SSMI pixel pairs when the TMI rain flag indicated rain.

In this case, there is substantially more scatter than under the no-rain conditions. The over-ocean and over-land pixel separation is still evident in the 19 GHz figures, with more scatter amongst the over-ocean pixels. At 85 GHz, up to 50K differences are noted between the TMI and the SSMI for the coldest 85 GHz pixels, and the difference falls off towards zero as the 85 GHz brightness temperature increases towards 260-270K. By averaging into the nearest 1-degree bin, much of this scatter could be reduced. However, in the GPM era, one of the goals is to produce rainfall products at sub 1-degree spatial scales (as fine as 0.1 degrees), which is approximately the same as the maximum allowed spatial offset used when collecting these data. For some of the finer-spatial and temporal scale GPM products, the product will be created from a small number of constellation overpasses, each taken with a different view of the underlying three-dimensional structure of the precipitating cloud.

Figure 6 depicts the TMI-SSMI difference as a function of the underlying TMI 2A12 rainfall rate. At 19 GHz, the trend is towards a positive difference as rainfall rate increases, which we believe to be attributable to the finer on-Earth FOV (i.e., better beamfilling) of the TMI 19 GHz channel versus that from the SSMI. However, at 85 GHz, where the surface is increasingly opaque, the TMI-SSMI brightness temperature difference trends towards zero (or slightly negative) as rainrate increases.

Figure 7 shows the TMI-SSMI difference as a function of the relative azimuth difference between the TMI and the SSMI. For relative azimuth near zero (i.e., where both sensors are viewing at nearly the same time and along the same 3-dimensional direction), there appears to be a minimum in the TMI-SSMI difference at 85 GHz. At 19 and 37 GHz, the TMI-SSMI difference is in many cases very large or very small, even near zero degrees relative azimuth difference.

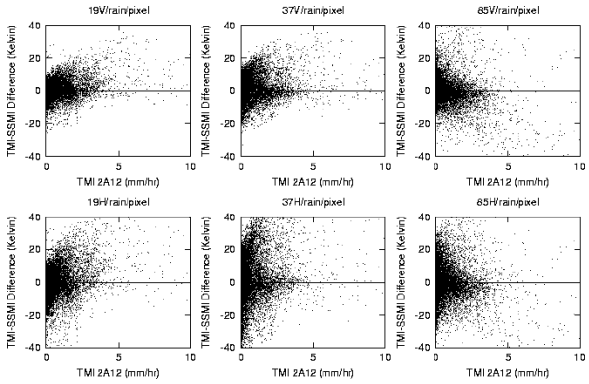

Figure 6. Scatter plot of the TMI-SSMI brightness temperature difference as a function of the TMI 2A12 rain rate.

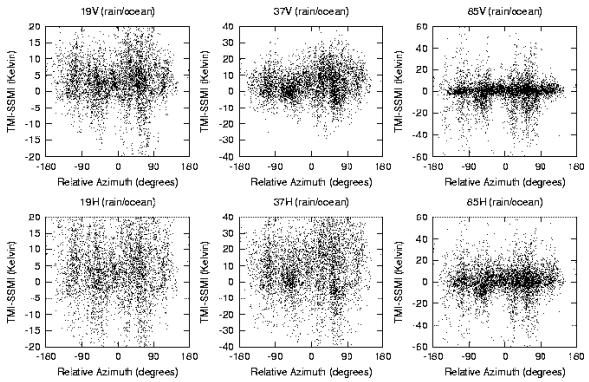

Figure 7. Scatter plot of the TMI-SSMI brightness temperature difference as a function of the relative azimuth difference (in degrees) between the TMI and SSMI viewing directions.

This shows that at all three frequencies, substantial brightness temperature differences are manifested over precipitating cloud. At 85 GHz, the difference is likely due to the different viewing directions and the ice water path optical depth along the viewing direction. At 19 and 37 GHz, the presence of clouds and the larger FOV make the comparison more difficult and conclusive. Larger FOV instruments such as the SSMI are more prone to beamfilling effects, whether the cloud is precipitating or non-precipitating. When collocated with smaller FOV instruments such as the TMI, the two observations are likely to contain a different percentage of cloud and surface.

3. CONCLUSIONS

We have presented the first results of a study of the nature of space and time collocated passive microwave observations from precipitating clouds. The data were taken from the TRMM TMI and the DMSP SSMI instruments during three months during November 2001 and February 2002, and respective pixels were collocated to within one-minute and 10-km in time and space, respectively. Further categorizing was done into over-land and over-water pixels (coastal pixels were rejected) and rain and no-rain conditions depending upon the TMI rain flag. While we only approximated the different sensor field of view and beamwidth characteristics with a simple 3x3 average of the TMI data, nevertheless the analysis permitted us to analyze the behavior of a GPM constellation that would sample (overpass) clouds on an intermittent time basis. To a first order, the results provide direct observations of the effect of three-dimensional clouds when viewed with a collection of passive microwave radiometers, each viewing from a different azimuthal direction. The comparisons at 19 and 37 GHz are hampered by the larger and different-sized FOV (different beamfilling), and so even with near coincident observations along the same three-dimensional direction there are substantial brightness temperature differences, both positive and negative.

Further investigations and data collections are ongoing with additional datasets collected over a long time period, and characterizing how the retrieved rain rates from the TMI and the SSMI compare when averaged over various space and time scales.

ACKNOWLEDGEMENTS

The first author gratefully acknowledges the support of his research sponsors, the Office of Naval Research, Program Element (PE-060243N) and the Oceanographer of the Navy through the program office at the Space and Naval Warfare Systems Command, PMW-155 (PE-0603207N).

REFERENCES

Bauer, P., L. Schanz, and L. Roberti, 1998: Correction for three-dimensional effects for passive microwave remote sensing of convective clouds. *J. Appl. Meteor.*, **37**, 1619-1643.

Bidwell, S.W., Yuter, S., Adams, W.J., Everett, D.F., Fleming, G.M., Smith, E.A., 2002: Plans for Global Precipitation Measurement ground validation. *Proc. Int. Geoscience Rem. Sens. Symp.*, Toronto, 24-28 June.

Fleming, G.F., 2002: Requirements for Global Precipitation Measurement. *Proc. Int. Geoscience Rem. Sens. Symp.*, Toronto, 24-28 June.

Haferman, J.L., W.F. Krajewski, T.F. Smith and A. Sanchez, 1993: Radiative transfer for a three-dimensional raining cloud. *Appl. Optics*, **32**, 2795-2802.

Hollinger, J.P., J.L. Peirce, and G.A. Poe, 1990: SSM/I instrument evaluation. *IEEE Trans. Geosci. Rem. Sens*., **28(5),** 781-790.

Smith, E.A., J. Adams, P. Baptista, D. Everett, M. Flaming, Z. Haddad, T. Iguchi, E. Im, C. Kummerow, 2001: Optimizing orbit-instrument configuration for the Global Precipitation Mission (GPM) satellite fleet. *Proc. Int. Geosci. Rem. Sens. Symp*. (IGARSS-2001), July 9-13, Sydney, Australia.

Vivekanandan, J., J. Turk and V.N. Bringi, 1991: Ice water path estimation and characterization using passive microwave radiometry. *J. Appl. Meteor*, **30**, 1407-1421.